Ultrastructure of cell trafficking pathways and coronavirus: how to recognise the wolf amongst the sheep

Neil, Desley; Moran, Linda; Horsfield, Catherine; Curtis, Elizabeth; Swann, Olivia; Barclay, Wendy; Hanley, Brian; Hollinshead, Michael; Roufosse, Candice

DOI:
10.1002/path.5547

Journal of Pathology
J Pathol 2020; **00:** 000–000
Published online 22 October 2020 in Wiley Online Library (wileyonlinelibrary.com) DOI: 10.1002/path.5547

REVIEW

Ultrastructure of cell trafficking pathways and coronavirus: how to recognise the wolf amongst the sheep

Desley Neil[1,2*], Linda Moran[3,4], Catherine Horsfield[5], Elizabeth Curtis[1], Olivia Swann[6], Wendy Barclay[6], Brian Hanley[3,4], Michael Hollinshead[7] and Candice Roufosse[3,4]

[1] *Department of Cellular Pathology, Queen Elizabeth Hospital Birmingham, University Hospitals Birmingham NHS Foundation Trust, Birmingham, UK*
[2] *School of Immunology and Immunotherapy, College of Medical and Dental Sciences, University of Birmingham, Birmingham, UK*
[3] *North West London Pathology, Imperial College Healthcare NHS Trust, London, UK*
[4] *Department of Immunology and Inflammation, Centre for Inflammatory Diseases, Faculty of Medicine, Imperial College London, London, UK*
[5] *Department of Histopathology, Guy's and St Thomas' NHS Foundation Trust, London, UK*
[6] *Department of Infectious Disease, Faculty of Medicine, Imperial College London, London, UK*
[7] *Department of Pathology, University of Cambridge, Cambridge, UK*

**Correspondence to: D Neil, Department of Cellular Pathology, Queen Elizabeth Hospital Birmingham, Mindelsohn Way, Edgbaston, Birmingham, B15 2GW, UK. E-mail: desley.neil@uhb.nhs.uk*

Abstract

The severe acute respiratory syndrome coronavirus 2 (SARS-CoV-2) pandemic has resulted in an urgent need to understand the pathophysiology of SARS-CoV2 infection, to assist in the identification of treatment strategies. Viral tissue tropism is an active area of investigation, one approach to which is identification of virus within tissues by electron microscopy of post-mortem and surgical specimens. Most diagnostic histopathologists have limited understanding of the ultrastructural features of normal cell trafficking pathways, which can resemble intra- and extracellular coronavirus; in addition, viral replication pathways make use of these trafficking pathways. Herein, we review these pathways and their ultrastructural appearances, with emphasis on structures which may be confused with coronavirus. In particular, we draw attention to the fact that, when using routine fixation and processing, the typical 'crown' that characterises a coronavirus is not readily identified on intracellular virions, which are located in membrane-bound vacuoles. In addition, the viral nucleocapsid is seen as black dots within the virion and is more discriminatory in differentiating virions from other cellular structures. The identification of the viral replication organelle, a collection of membranous structures (convoluted membranes) seen at a relatively low scanning power, may help to draw attention to infected cells, which can be sparse.

Keywords: SARS-CoV-2; coronavirus; COVID-19; ultrastructure; electron microscopy; cell trafficking pathways; endolysosomal pathways; nucleocapsid; crown

Received 23 June 2020; Revised 10 August 2020; Accepted 6 September 2020

No conflicts of interest were declared.

Introduction

In the wake of the severe acute respiratory syndrome coronavirus 2 (SARS-CoV-2) pandemic, clinicians and scientists from around the world have mobilised technologies old and new to bring light to the pathophysiology underpinning the many clinical manifestations of infection, collectively referred to as COVID-19 (coronavirus disease 2019). Clinical presentations are of varying severity, from asymptomatic to life-threatening, and often affect multiple organs. We do not yet fully know how much of the damage in each organ is related to direct viral cytopathic effect and/or to secondary pro-inflammatory and/or pro-thrombotic injury. In-depth analyses of tissue samples from living patients and post-mortem examinations are key to deciphering the relative contribution of these events and guiding the development of effective therapies.

SARS-CoV2 can be identified within each organ through detection of its proteins and RNA. The specific cell types infected can be determined by spatial profiling or single cell analysis. Electron microscopy (EM) has also been used to identify virions within tissue. Indeed, human coronavirus was first described by virologist June Almeida in 1967, then at St Thomas' Medical School in London, through the use of negative staining electron microscopy on human nasal and tracheal epithelial cells grown in culture and infected with 'nasal washings from a patient with a cold' [1]. Almeida and colleagues named the new virus coronavirus, because of its appearance in these original photographs, 'recalling the solar corona'

[2]. Since then, in several coronavirus outbreaks (SARS [3], MERS [4], and the current SARS-CoV-2), intracellular and extracellular structures with a corona have been used to suggest the purported presence of virus in a variety of tissues (upper and lower respiratory tract, large intestine, kidney, and macrophages), when they are in fact showing structures associated with cell trafficking pathways. Many of the observations have been made on poorly preserved autolysed post-mortem tissues. In addition, exposure to EM technique and interpretation is limited in routine diagnostic histopathology practice and largely confined to renal and neuromuscular pathology. Therefore, intimate knowledge of ultrastructural human cell substructures is not widespread amongst pathologists. The advent of super-resolution microscopy, which allows near-EM resolution immunofluorescent imaging, has led to major advances in understanding the normal cellular trafficking pathways relevant to viral entry, replication, and release [5]. Diagnostic pathologists are not up to date with these advances. Clathrin-coated vesicles, caveoli, and multivesicular bodies have been misinterpreted as being cytoplasmic coronavirus particles because these structures have the appearance of being coated with 'spikes' [6–9]. These are, in fact, part of normal cell trafficking pathways. The confusion has been caused by a lack of integration of basic science and virology into clinical pathology, where there is limited appreciation of other structures with 'crowns' and limited knowledge of the effect of staining and processing on the visibility of the coronavirus 'crown'.

The aim of this review is to help in the differentiation of the 'normal' cell from a coronavirus-infected cell, by providing an update on the dynamic ultrastructure of cell trafficking pathways, with a particular emphasis on intracellular and extracellular features that could be confused with virions. Additionally, the more typical features of a coronavirus on routinely processed clinical electron microscopic samples are described.

Ethics

Anonymised diagnostic electron micrographs were reviewed randomly for good illustrations of the cell trafficking structures. Electron microscopy samples from human subjects were obtained from the Imperial College Healthcare NHS Trust Tissue Bank (MREC 17/WA/0161) (approved project number R20012). QEHB and GSTT/KCH: no specific ethics as not patient identifiable.

Cell trafficking and secretory pathways as ultrastructural 'mimics' of SARS-CoV-2

Proteins and other molecules, collectively termed cargo, are transported around the cell in a highly orchestrated manner, with membrane-bound vesicles as 'carts' and the microtubular system as 'tracks' [10]. There are two main sites of sorting and packaging of proteins and other molecules in the cell: the endosome [11] and the outer layer of the Golgi apparatus called the trans-Golgi network (TGN) [12]. A third possible site of sorting, predominantly in cells of haematopoietic lineage, occurs in the lysosomes [13]. The endosome deals with proteins internalised by endocytosis and from the TGN, whereas the Golgi deals with proteins from the endoplasmic reticulum, endosomes, and lysosomes. The endoplasmic reticulum (ER)–Golgi intermediate complex (ERGIC) transports proteins from the ER to the Golgi and returns proteins that fail quality control back from the Golgi to the ER [14].

Endocytosis

Endocytosis is the process of transport of a 'cargo' from the extracellular surface of the cell to its inside; the cargo consists of extracellular ligands and their transmembrane proteins, including soluble molecules, protein, and lipids. Endocytosis takes place at the cell membrane by a number of routes [15–17] (Figure 1), of which the two main pathways are clathrin-mediated endocytosis (Figure 2A) and caveolin-mediated endocytosis (Figure 2A). Caveoli, clathrin-coated pits (CCPs), and clathrin-coated vesicles (CCVs) were identified over 50 years ago with the advent of EM. Both pathways require the cell membrane to bend and pinch off from the plasma membrane, leading to single membrane-bound vesicles; this is achieved by external coating of the vesicles with membrane-associated proteins, followed by actin polymerisation and enzymatic separation (scission) from the donor membrane [17,18]. Clathrin-mediated endocytosis starts with CCPs 60–120 nm in diameter [17], which are readily identified by the clathrin scaffold on the surface facing the cell cytoplasm, which imparts a distinct bristle coat [19]. After internalisation, the clathrin coat is removed from the CCVs (Figure 2B). Multiple receptors, such as those for insulin and transferrin, are involved with the clathrin-mediated pathway [16,20]. Caveolin-mediated endocytosis occurs via specialised lipid rafts that form 50–100 nm flask-shaped invaginations (caveoli) of the plasma membrane. Caveolin-rich lipid rafts initiate the process, with cavin proteins coating the cytosolic side of the membrane [16,20]. Other pathways are termed clathrin-independent endocytosis and are not readily identified by EM.

The endolysosomal pathway

Upon internalisation, the cargo in the endocytic vesicle enters a complex trafficking pathway. Some vesicles are transported across the cell (transcytosis); this occurs predominantly after caveolin-mediated endocytosis [16,20,21]. Most endocytic vesicles are quickly targeted to the early endosome (EE) (Figure 3), a sorting station, where the fate of the cargo is determined. The exact mechanism by which an EE forms is unclear; however, the membrane volume is mainly derived from the fusion of endocytic vesicles from all pathways [24]. EEs tend to be peripherally placed in the cells, close to the plasma membrane [24], and have a complex pleomorphic structure (Figure 3B), varying between cell types. The EE can

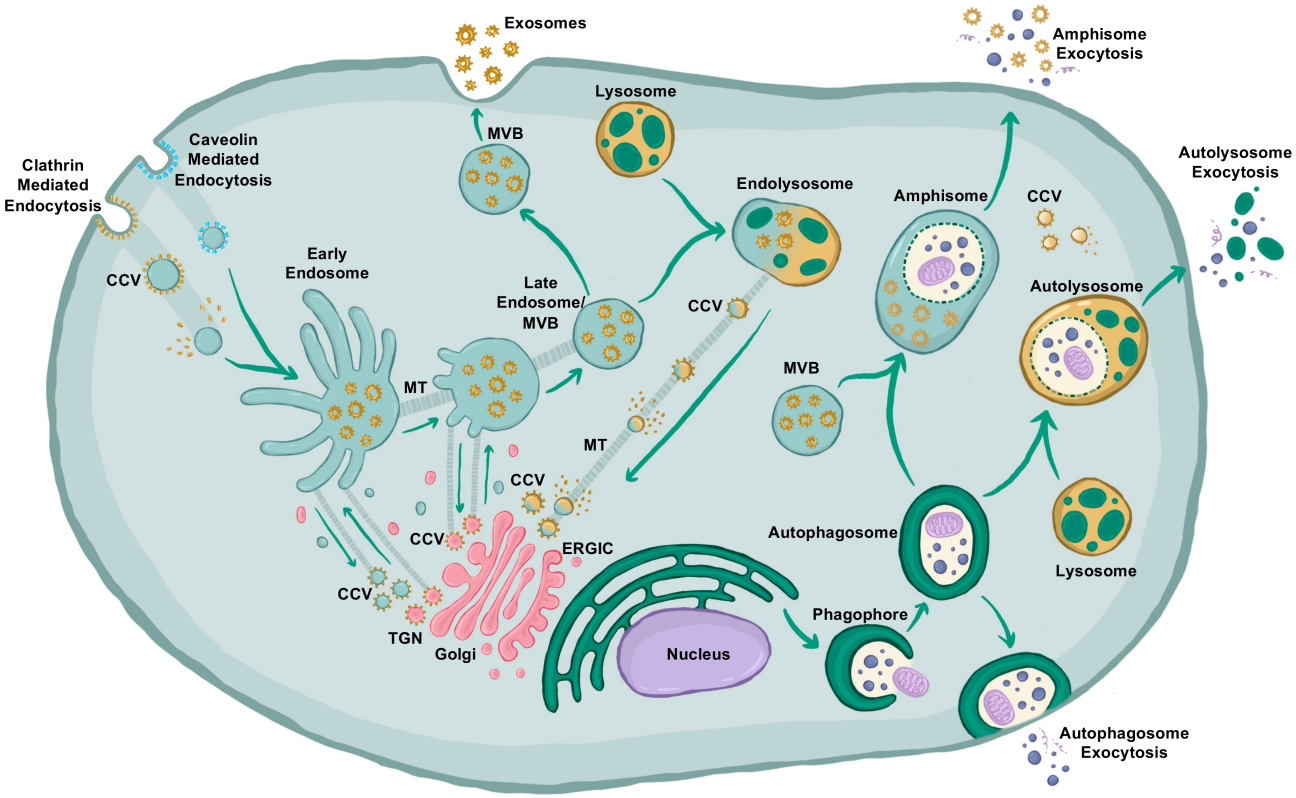

Figure 1. Cell trafficking pathways. Endocytic entry to the cell is via clathrin-coated pits, caveoli or clathrin-independent endocytosis (not shown, as not identifiable by EM). The 'spikey' clathrin coat (yellow dots) is removed from the clathrin-coated vesicles (CCVs) after endocytosis. CCVs and caveoli-derived endocytic vesicles are incorporated into the early endosome (EE), which has tubular extensions and a bulbous part in which there are microvesicles. CCVs predominantly bud off the EE; the contents are either recycled to the cell membrane or transported to the *trans*-Golgi network along microtubules (MT). The EE, moving along MTs, matures into the late endosome (LE), which is mostly derived from the bulbous part of the EE and is termed a multivesicular body (MVB) containing intraluminal vesicles (ILVs). The MVB may (1) be transported along microtubules to the cell membrane and the ILVs released by exocytosis as exosomes; (2) fuse with a lysosome to form an endolysosome or (3) fuse with an autophagosome to form an amphisome. Lysosomes contain enzymes for breakdown of the cargo. CCVs are released from the lysosomal-derived structures (endolysosome, autolysosome) and transported to the Golgi apparatus for further sorting or to the cell membrane for release by exocytosis. In addition, a clathrin coat is present on many of the intraluminal vesicles within the endolysosomal system, obtained during internalisation.

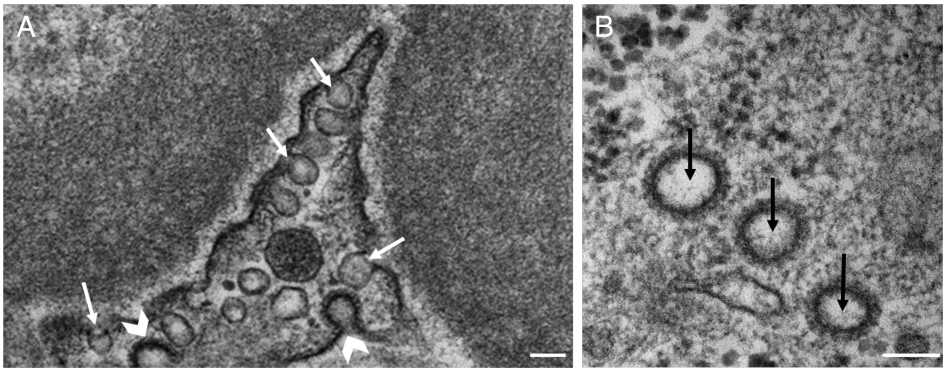

Figure 2. Endocytic pathways. (A) Glomerular mesangial cell with caveoli (arrows) and clathrin-coated pits (arrowheads). Scale bar = 100 nm. (B) Podocyte containing clathrin-coated vesicles (arrows). Scale bar = 100 nm.

have both thin tubular extensions approximately 60 nm in diameter and bulbous areas 400 nm in diameter with membrane invaginations (Figure 1). The membrane invaginations in bulbous areas impart a multivesicular appearance on transverse section (Figure 3A,C) [25,26]. Proteins targeted for recycling are directed to the tubular extensions, whereas the multivesicular area is usually involved in sorting proteins towards the degradation pathways, with the involvement of ubiquitin [22,27].

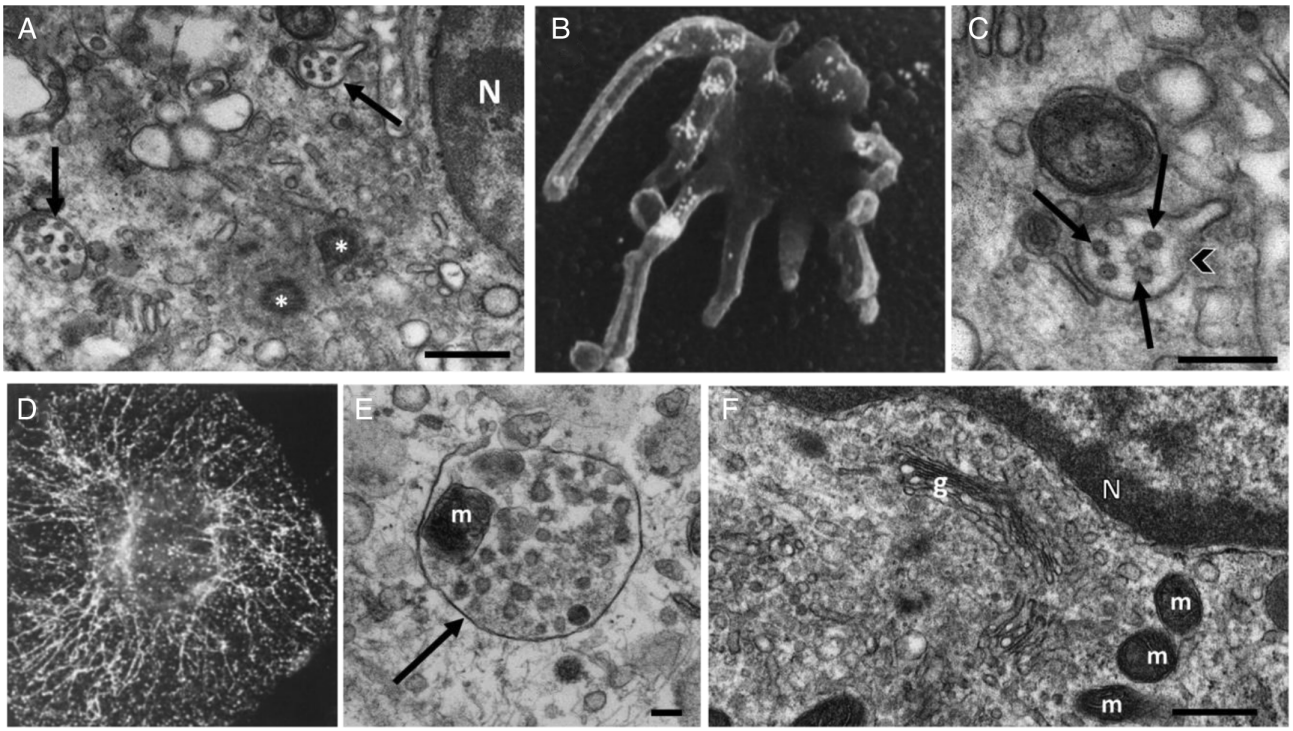

Figure 3. Cell trafficking structures. (A) Podocyte containing multivesicular bodies (arrows) and microtubular organisation centres (*). N, nucleus. Scale bar = 500 nm. (B) Freeze etch electron micrograph on an early endosome illustrating the tubular network. The endosome is visualised by low-density lipoprotein (LDL)-gold particles endocytosed for 5 min (gold particles are visualised as white spots). Reproduced from [22] with permission. (C) Higher magnification of an overlapping field of panel A showing a multivesicular body (MVB) (arrowhead) containing intraluminal vesicles (arrows) with a clathrin coat, giving a spikey appearance. A tubular process can be seen extending from the MVB. Scale bar = 250 nm. (D) Network of long tubular endosomes in HeLa cells incubated for 5 min in 5 μg/ml brefeldin A. Reproduced from [23] with permission. (E) An autolysgosome/amphisome (arrow) in a podocyte containing a mitochondrion (m) for degradation and vesicles with a spikey clathrin coat. Scale bar = 100 nm. (F) Podocyte with a Golgi apparatus (g) with numerous cell trafficking microvesicles nearby. m, mitochondrion; n, nucleus. Scale bar = 500 nm.

The network of endosomal tubules can be remarkably extensive [28] (Figure 3D). Endocytosed receptors are recycled to the cell membrane [27] via a fast or slow pathway [25,29]. Fast recycling involves direct transport to the plasma membrane, whilst the slow route involves a system of semiautonomous or interconnecting recycling membrane pathways [23], together generally termed the recycling endosomes (REs). REs are transported along microtubules to a perinuclear position, where they cluster in the endocytic recycling compartment adjacent to the microtubule-organising centre (MTOC)/centriole [25]. They are involved in transport to and from the TGN [30]. Recent evidence suggests that cargo recycling is highly regulated, requiring endosomal sorting complexes, and that several of these processes are regulated by actin [29].

The bulbous areas of the EE containing the intraluminal invaginations mature into multivesicular bodies (MVBs) or late endosomes (LEs). MVBs (Figure 3A, C), recognised since the advent of EM, measure 100–1000 nm in diameter and contain intraluminal vesicles (ILVs) approximately 50–100 nm in diameter [22,24]. ILVs are predominantly produced by a clathrin coat mechanism [31]. Protein (cargo) tagged with ubiquitin is targeted to the MVB [22]. The MVB may fuse with the cell membrane and release the ILVs as exosomes into the extracellular environment (Figure 1) [22], or may fuse with a lysosome, which contains enzymes for degradation [22,32] (Figure 1). LEs/MVBs may also fuse with autophagosomes (Figures 1 and 3E) to form an amphisome [33]. Autophagosomes are formed during autophagy (Figure 1), a process of degradation and recycling of cellular components. In autophagy, an omegasome arises from the ER [34] and forms a tubular structure, a phagophore (Figure 1), which wraps around and encloses the material to be degraded, forming the autophagosome (Figure 1), which by virtue of this process has a double membrane. Therefore, when an LE/MVB fuses with an autophagosome, it may for a period have a double membrane, prior to fusing with a lysosome to form an autolysosome (Figure 1) [33,35]. Further sorting of cargo occurs in the lysosome/lysosomal fusion structures (Figure 1); proteins not for degradation are released as vesicles via clathrin pathways [36,37] or by exocytosis [33].

The Golgi apparatus

The Golgi apparatus (Figures 1 and 3F) is a sorting system for proteins from the ER, endosomes, and lysosomes. It is composed of a variable number of layers of

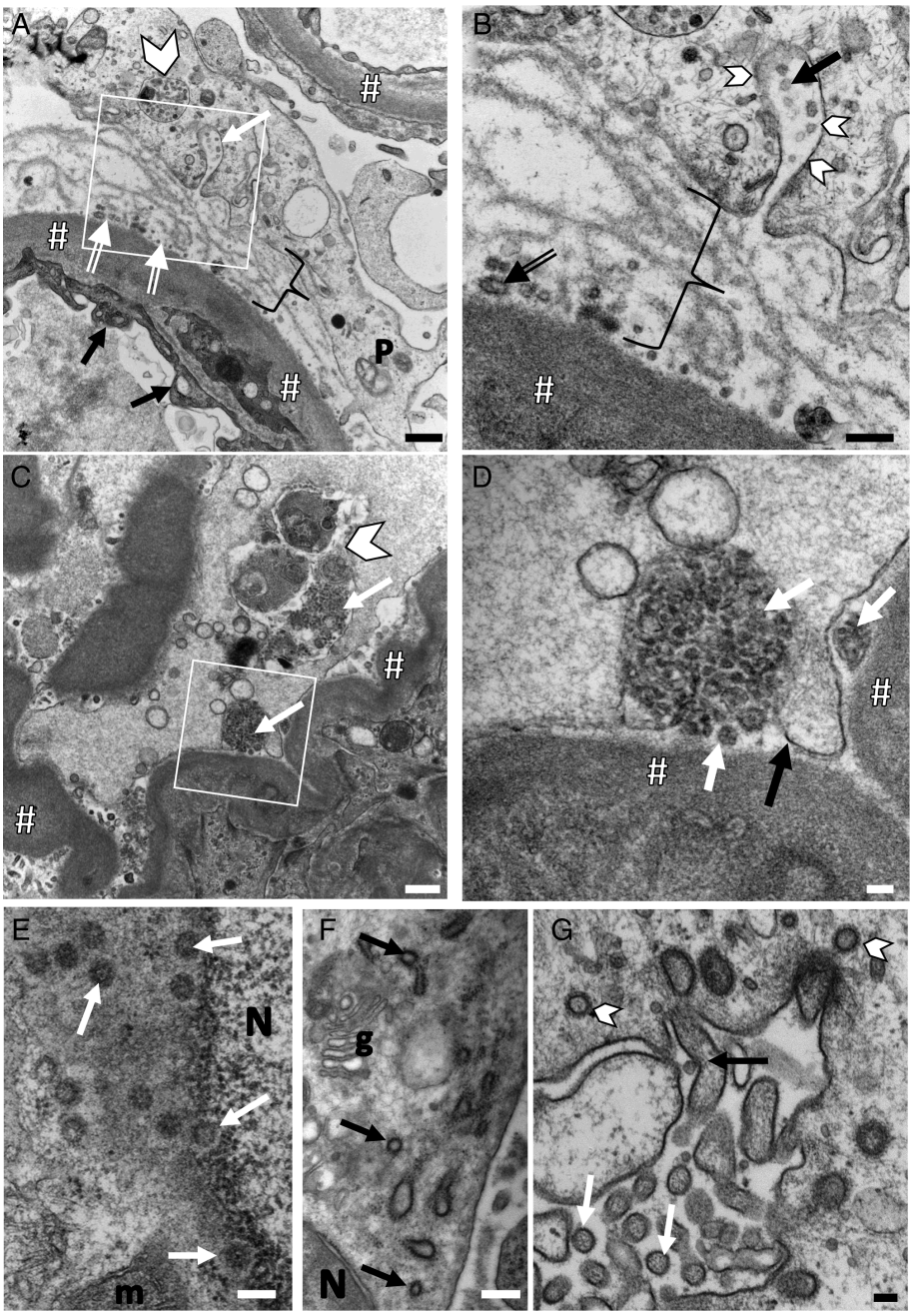

Figure 4. Exocytosis/extracellular vesicles and other mimics. (A) Podocyte (P), glomerular basement membrane (#), and glomerular endothelium (black arrow). There is an autolysosome/amphisome (arrowhead) (same as Figure 3E) and exosomes (white arrow). Extracellular vesicles (split white arrow) are also seen within reduplicated subepithelial basement membrane (}). Scale bar = 500 nm. (B) Higher power of the exocytotic vesicles in the boxed area in A. Plasma membrane (arrowhead), exosomes (black arrow), extracellular vesicles (split arrow), glomerular basement membrane (#), and replicated subepithelial basement membrane (}). Scale bar = 250 nm. (C) Podocyte containing an autolysosome (arrowhead); some of the contents are granular (arrow). Similar granular material is seen outside the cell, having been exocytosed (arrow in the box). Scale bar = 500 nm. (D) Higher power of the exocytosed membrane-bound vesicles (white arrow) from the boxed area in C. Black arrow indicates plasma membrane. Scale bar = 100 nm. (E) Edge of a nucleus (N) near which nuclear pores (arrows) are forming round structures with a granular texture and slightly spikey appearance. m, mitochondria. Scale bar = 250 nm. (F) Podocyte containing rough endoplasmic reticulum (arrows) which could be confused with coronavirus due to the 'spikey' appearance of the ribosomal coat. Golgi apparatus (g) and nucleus (N) are present. Scale bar = 250 nm. (G) Microvilli (black arrow) can be seen extending from the cell surface. Where cut in transverse section (white arrow), they look similar to coronavirus, with a textured dotty interior and dense, slightly spikey outer layer. Clathrin-coated vesicles (arrowheads) are present within the cytoplasm and have a similar appearance. Scale bar = 250 nm.

cisternae. The layer nearest the ER receives vesicles containing proteins and lipids from the ER and is known as the *cis*-Golgi network (CGN) or the ERGIC. The layer furthest away from the ER is the TGN, and collects, sorts, and packages numerous molecules within vesicles for transport to their final destination [12]. Clathrin and other coated pits are involved in the secretion of vesicles from the TGN [12,38].

Exocytosis

Extracellular vesicles (Figure 4) comprise vesicles with a membrane derived either from organelle membranes (exosomes) or from the plasma membrane (microvesicles) [25,39]. Exosomes can be formed by the fusion of an MVB with the plasma membrane and release of the ILV as exosomes. They measure 30–150 nm in diameter, whereas microvesicles can measure 30–1000 nm in diameter [40]. Extracellular vesicles contain cellular proteins, RNA, and DNA, and can endocytosed by other cells, allowing cross talk between cells [40,41].

Other potential ultrastructural coronavirus 'mimics'

Another potential intracellular mimic is the nuclear pore. The nuclear pore is a tubular structure that passes across both nuclear membranes projecting into the nucleus and cytoplasm either side, allowing the transport of proteins, mRNA, tRNA, and ribosome subunits. Nuclear pores are 80–120 nm in diameter, with an inner diameter of approximately 40 nm [42]. Because they project beyond the nuclear membrane, they may appear as a round structure distinct from the nucleus on TEM (Figure 4E). The rough ER (Figure 4F) has ribosomes attached to the membrane forming projections that have also been confused with the spikes of coronavirus [9].

Transverse sections through microvilli may be confused with extracellular coronavirus. Microvilli are cellular membrane protrusions that are involved in a wide variety of cellular functions. They are made of a single plasma membrane and inside cytoplasm with microfilaments (e.g. actin and others) but no organelles. Microvilli measure 50–100 nm in diameter on cross-section and are covered with a glycocalyx, which can show spiky extensions on EM, giving the appearance of a 'crown' (Figure 4G) [43,44].

Coronavirus structure, replication, and ultrastructural appearances

Much of our current understanding of cell infection with SARS-CoV-2 relies on previous work done with SARS-CoV, the agent that caused the SARS outbreak in 2002–2004. The genome sequences are 79.5% identical, with 86% non-structural protein sequence identity; it is thus considered highly likely that the replication process of both viruses is similar [45].

Both SARS-CoV and SARS-CoV-2 are enveloped RNA viruses. Their membrane is acquired from host membranes and therefore has a similar ultrastructure, i.e. a lipid bilayer. Viral membrane (M), envelope (E), and spike (S) proteins are embedded within this membrane when the virus is formed in host cells, with the S proteins projecting from the surface to appear on negative staining EM as a crown (corona) [46,47]. The nucleocapsid, consisting of the viral RNA and associated with nucleocapsid (N) protein, is located within this envelope (Figure 5).

Coronaviruses all induce similar replicative structures within cells. They replicate in the cytoplasm, in conjunction with modified endomembranes derived from the endoplasmic reticulum forming the viral replication organelles (ROs) (Figure 6B,C), without nuclear involvement [45,49]. Figure 5 depicts the intracellular viral replication pathway, which we describe in more detail here. The initiation of cell entry involves binding of the receptor binding domain of the S protein to the protease domain of angiotensin-converting enzyme 2 (ACE2), which acts as a receptor [50–54]. Whilst exact mechanisms for cell entry of SARS-CoV-2 are not yet known, they are likely to be similar to SARS-CoV, in which clathrin-dependent [45] and clathrin-independent [55] endocytosis pathways are used; the pathway involved may vary between cell types [56]. Using a SARS-CoV-2 pseudovirus model, cell entry was found to be mainly by clathrin-dependent endocytosis [51]. The endocytosed virus enters the endocytic pathways of the cell and is delivered to an endosome [57], resulting in the intact virion within an endocytic clathrin-coated vesicle. The virion envelope fuses with the endocytic vesicle/EE membrane, releasing the uncoated viral nucleocapsid into the cytoplasm.

Translation of the viral genomic RNA results in two polyproteins that are proteolytically cleaved to form non-structural proteins (NSPs), which induce the RO [45]. The RO comprises convoluted membranes, double membrane vesicles (DMVs) [45,58–61], and small open double membrane spherules, all derived from, and remaining connected to, the ER, which may include zippered areas [45,62]. DMVs are common to all coronaviruses, whilst the other structures may not be [45]. The replication transcription complexes (RTCs), the virus replication machinery, produced by transcription of the viral genomic RNA, are anchored to these membranous structures [60,61]. The RTCs facilitate further transcription of a subset of sub-genomic RNA, which occurs within the DMVs. The sub-genomic RNA encodes for 15–16 viral structural and accessory proteins. Translation of the membrane structural and accessory proteins occurs in the ER, whilst translation of the N proteins occurs in the cytoplasm on free ribosomes [48]. Complete copies of the genomic RNA are replicated from a negative copy of the genomic RNA in the cytoplasm [48]. The translated membrane structural proteins move along the ER secretory pathway to the ERGIC, where partial assembly of the viral envelope proteins occurs [48]. The viral genomes encapsidated by N proteins butt into the ERGIC partial viral envelope, forming a bud in the ERGIC, which pinches off, resulting in virions within cisternal spaces derived from the Golgi/ER [48,63]. The virions within vacuoles are transported to the cell membrane, using the usual secretory route of the ER/Golgi complex [64], and released by exocytosis [48,65].

Ultrastructural viral features have been described based on images from infected cultured cells, where they measure 60–140 nm in diameter with spikes 9–12 nm in length [64], the spikes being seen on

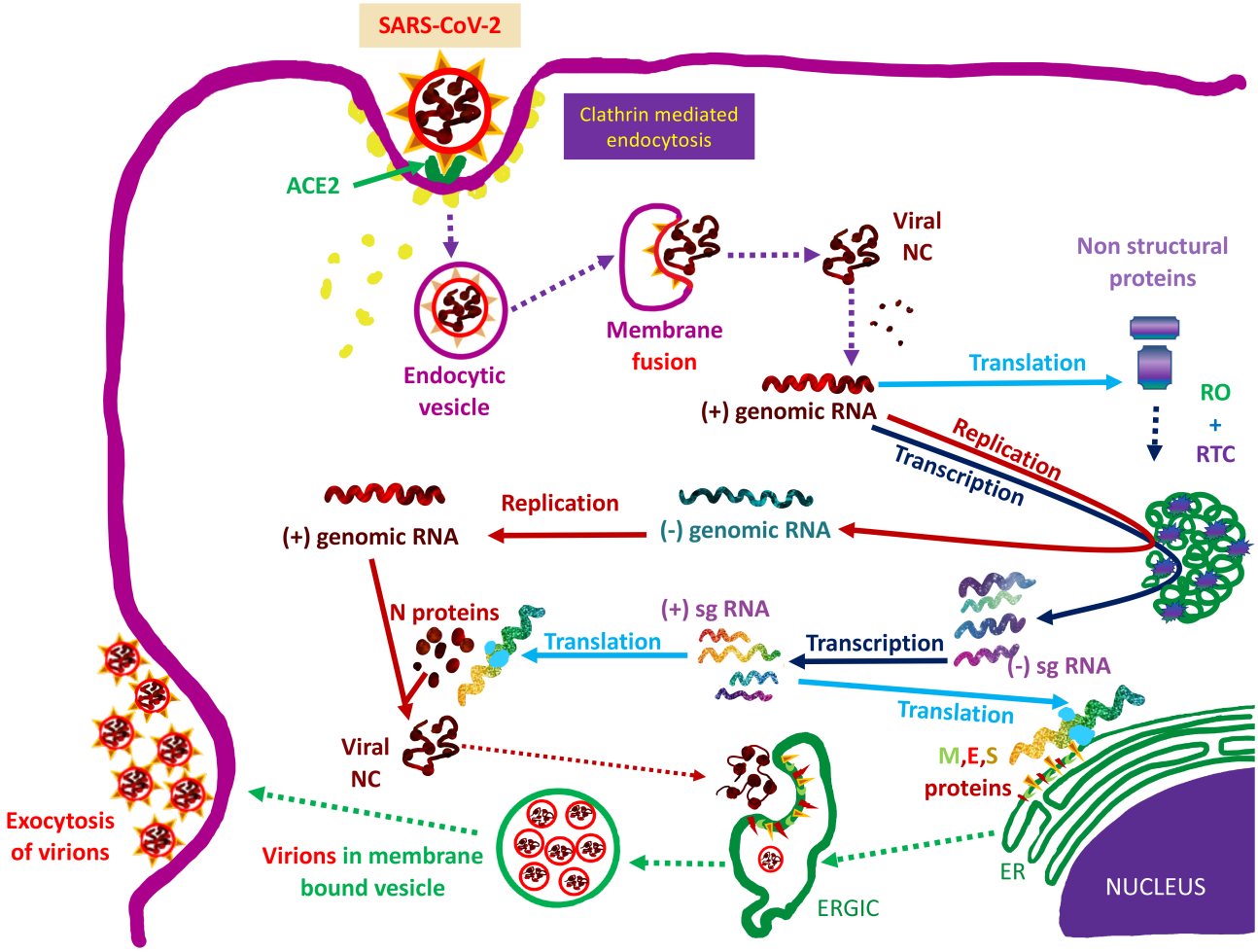

Figure 5. Viral replication pathways. SARS-CoV-2 binds ACE2 on the cell membrane and enters the cell via clathrin-mediated endocytosis. The virion membrane fuses with the endocytic membrane with release of the nucleocapsid (NC) into the cytoplasm. The free genomic RNA is then translated and cleaved to non-structural proteins, which induce the formation of the replication organelle (RO), comprising endoplasmic reticulum (ER)-derived membranous structures in which the replication transcription complex (RTC) proteins are embedded. Replication of genomic and subgenomic (sg) RNA, via a negative sense RNA, occurs in the replication organelle. Translation of the nucleocapsid proteins (N) occurs on cytosolic ribosomes, and translation of the envelope (E), membrane (M), and spike (S) proteins occurs on rough ER, with insertion of these proteins into the ER membrane. The N proteins associate with the genomic RNA to form the nucleocapsid, which then buds into the ER–Golgi intermediate complex (ERGIC). The resultant vesicle buds off into the ERGIC, forming a virion with the envelope acquired from the ERGIC membrane in which the E, M, and S proteins are embedded. Virions are transported to the cell surface in membrane-bound vacuoles and released by exocytosis. Adapted from [48,49].

negatively stained specimens. Coronaviruses at different stages of development can be found in membrane-bound vacuoles within the cytoplasm of the infected cell [66], or outside the cell, near the plasma membrane [64] (Figure 6C–F). The helical viral nucleocapsid produces characteristic black dots within the virion [9,67,68] (Figure 6F).

Transmission EM on human tissue to identify virus: how do you recognise a wolf in sheep's clothing?

EM of diagnostic tissue sections is not an easy option for the identification of virus and there is limited experience in this field: The subset of histopathologists who use EM are not usually required to identify viruses, whereas virologists, who rarely use EM or use EM only on optimally preserved viral or cell preparations with different techniques (e.g. negative staining), are not used to poorly preserved and suboptimally handled diagnostic tissue samples [66,69,70]. Most EM related to coronaviruses is undertaken in animal/veterinary research facilities, with little translation into the clinical diagnostic field. In addition, there are differences between the ultrastructural features of infected tissue culture cells and infected cells *in vivo* [67]. For example, DMVs and nucleocapsid may be harder to identify in post-mortem and surgical samples [67] and may only be present at very low quantity. Taking all of these factors into account, it is perhaps not surprising that errors in interpretation of clinical EM samples have been made both in the current coronavirus outbreak [6–9] and in previous outbreaks affecting humans [3,4].

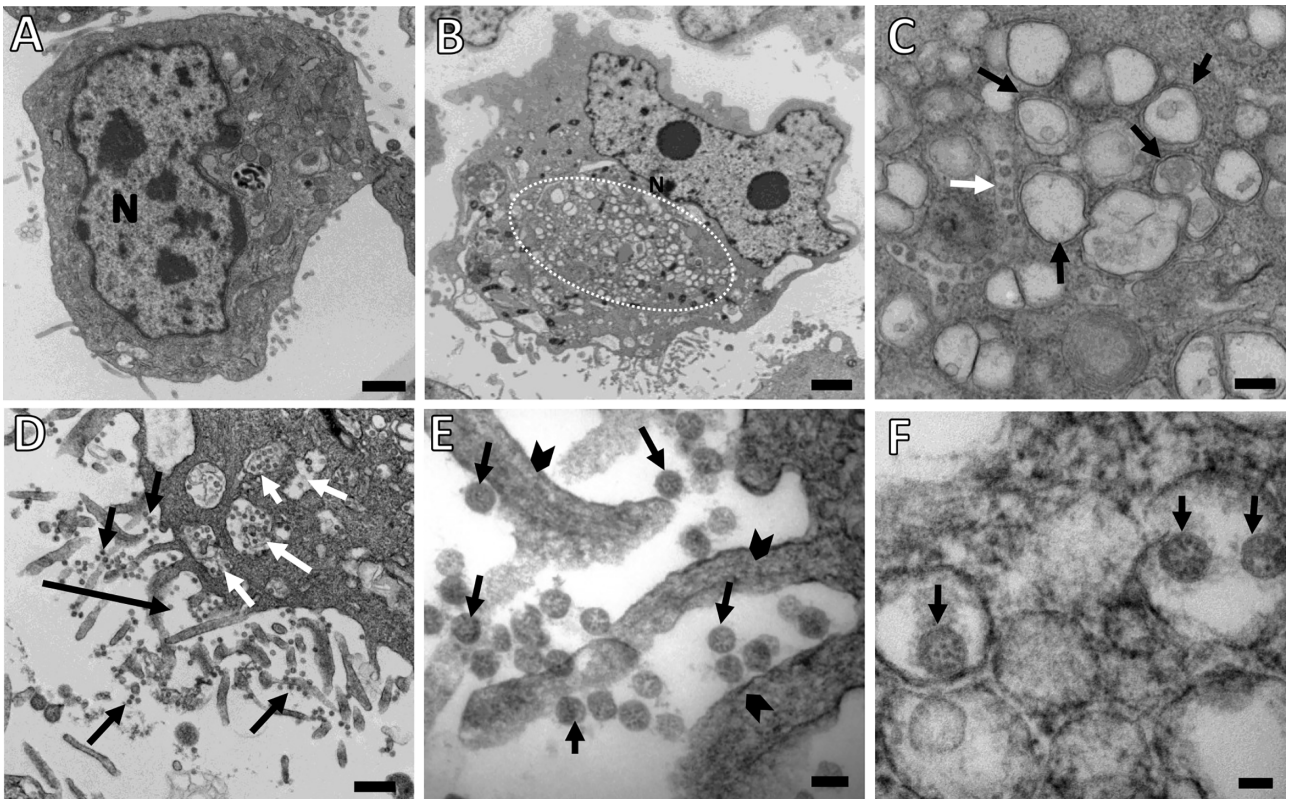

Figure 6. SARS CoV-2-infected Vero E6 cells. (A) Control mock-infected (bar = 1 μm) and (B–F) infected with SARS-CoV-2. Cells were infected at a multiplicity of infection of 0.1 and fixed 48 h post-infection in 3% glutaraldehyde in sodium cacodylate buffer. (B) Infected cells contain dilated membrane-bound structures in the cytoplasm – the replication organelle (dotted oval) – which may aid detection of infected cells at low power. This may be less conspicuous in biopsy and post-mortem specimens. Scale bar = 2 μm. (C) The replication organelle derives from the endoplasmic reticulum and is largely composed of double-membrane vesicles (black arrows). An elongated membrane-bound structure containing virions with a 'peas in a pod' appearance (white arrow) is present. Scale bar = 200 nm. (D) Numerous virions are seen as small round particles within membrane-bound vacuoles (white arrows) in the cytoplasm and extracellularly closely associated with the microvilli (black arrows). Scale bar = 600 nm. (E) Higher magnification showing the extracellular virions (arrows) with a dotty salt-and-pepper appearance due to the internal nucleocapsid, amongst microvilli (arrowheads). The 'crown' is not apparent in this preparation. Scale bar = 100 nm. (F) Intracellular virions (arrows) within single membrane-bound vacuoles. The nucleocapsid provides the characteristic dots within the virion and the phospholipid bilayer of the viral envelope similar to the vacuole membrane can just be distinguished. No definite crown (spikes) are seen, which is usually the case on intracellular virus unless special processing is undertaken. Scale bar = 50 nm.

The type of tissue and processing pathways can alter the size and appearance of the virus. SARS-CoV-2 is smaller when tissue is taken from a formalin-fixed, paraffin-embedded block, averaging 75 nm, compared with 105 nm in diameter when tissue is processed directly for electron microscopy [67]. Using routine diagnostic EM processing techniques, intracellular virus lacks prominent spikes, whilst they may be visible on extracellular virus [67]. This is because the appearance of surface glycoproteins can be lost during routine processing, and the spike is a glycoprotein [46,71]. Tannic acid pretreatment during processing can enhance visualisation of the spikes [72].

Infected cells can be sparse and therefore unsampled in small diagnostic tissue samples, contrary to optimised cell cultures. Intracellular trafficking structures can be easily confused with the virus. To improve certainty that a structure is of viral origin, immunoelectron microscopy and ultrastructural *in situ* hybridisation can be performed [72]. Immunoelectron microscopy involves a primary antibody to a specific viral protein, detected with a secondary antibody labelled with gold, which is electron-dense. Standard glutaraldehyde and paraformaldehyde fixatives with uranyl acetate and lead citrate staining may be compatible with this technique, although this depends on the antibody. However, osmium tetroxide post-fixation may interfere [73]. In immunoelectron microscopy experiments, a much lower percentage of glutaraldehyde is usually used to optimise the antigen. Tissue embedded in acrylic resin rather than the standard epoxy resin will result in better antigen preservation, related to low-temperature polymerisation [73]. Ultrastructural *in situ* hybridisation uses negative sense riboprobes and is best accomplished on tissues in a hydrophilic acrylic resin [72]. However, these techniques are complicated and not usually available in a diagnostic histopathology department.

While we await the results of these complex investigations, the following points may help to establish if an intra- or extra-cellular structure likely represents a virus.

- Virally infected cells may not be numerous; in general, beware of viral-like structures that are present in all the cells visualised. Compare any structures with

a negative control matched sample (same tissue, similar disease, with identical sample processing) from patients known not to be infected.
- Consider biological plausibility when considering which cell types might be infected; ACE2 acts as the receptor for cell entry by SARS-CoV-2 [54]. ACE2 is expressed on arterial and venous endothelial cells throughout the body [54] (with the exception of liver sinusoidal cells and glomerular endothelial cells [74,75]), arterial smooth muscle cells, ciliated epithelial and goblet cells in the upper airways, type I and II pneumocytes in the lung, biliary epithelial cells [76,77], podocytes and parietal epithelial cells [77], proximal renal tubular epithelial cells, gut epithelial and smooth muscle cells, cardiac myocytes, epicardial adipocytes and fibroblasts, pigmented epithelial cells, rod and cone photoreceptor cells in the eyes, and neurones and glial cells in the central nervous system [78]. Molecular and/or immunohistochemical investigations have provided evidence for SARS-CoV-2 in a limited number of cell types. The highest levels of viral protein and/or RNA are detected in alveolar pneumocytes and ciliated bronchial epithelial cells [67,79–84]. In a subset of patients deceased with COVID-19, lower amounts of virus have also been identified in the epithelium of the gastrointestinal tract [82], biliary epithelium [82], renal tubular epithelium [82,83], glomerular cells [84], and alveolar macrophages and alveolar capillary endothelial cells [82]. In other cases, viral RNA has been found in tissues without data on specific cell types infected: heart [79,82,84,85], skeletal muscle [82], lymph nodes [79], and brain [83]. In patients with skin lesions, the virus has been identified in endothelium of the vessels within the skin [86].
- Low-power magnification may help to identify the sparse infected cells. The viral replicative organelle results in an excess of membrane-bound spaces within the cell compared with neighbouring cells which may be visible at low power (Figure 6B). Based on molecular data, infected cells tend to be clustered [82]. If identified, the RO is a useful clue to viral origin.
- In cases where the RO is only present in low quantity, medium-power magnification may help to identify the sparse infected cells by the identification of accumulating virion in membrane-bound vacuoles (Figure 6D).
- Intracellular virus is found in membrane-bound structures, mostly in the cisternae of the ER–Golgi after replication and membrane-bound vacuoles transporting the virions to the cell surface and briefly in endocytic vesicles after cell entry; intracytoplasmic structures with a 'corona' directly projecting into the cytoplasm (rather than into a cisternal space) are likely CCVs [7], derived from endocytosis, from the TGN or from endosomes/endolysosomes.
- Cross-sections through the viral nucleocapsid result in black dots within the viral particle (Figure 6E,F) [9,67]. A membrane-bound structure containing virus-sized structures but without these internal dots is likely a normal endolysomal structure, most commonly an MVB, but could also be an endolysosome, amphisome or autolysosome.
- Infected cells tend to have both intracellular and extracellular virus (Figure 6D), as the virus will be replicating
- Extracellular virus, often with spikes as well as the characteristic nucleocapsid dots, is seen along the cell membranes and amongst cilia/microvilli [67].
- Both intracellular and extracellular virus show relative uniformity in size compared to endosomal structures.

Summary

Cells have a system for sorting and transporting 'cargo', centred on the endosomal network, with bidirectional connections between the cell membrane, lysosomes, Golgi, and ER. The endosomal network is a system of tubules and microvesicles which derive from the early endosome formed from endocytic vesicles, which matures to the late endosome/multivesicular bodies. At the ultrastructural level, these structures are being confused with a coronavirus when they have a coat which gives a spikey 'crown-like' appearance. A coat, most commonly clathrin, is required to allow membranes to bend to form vesicles, so CCVs are fairly ubiquitous throughout all cell types. However, the spikes on coronavirus virions are not readily identified on routinely prepared TEM samples; inner 'dots' representing nucleocapsid are the more characteristic feature in tissue samples. A useful clue to identifying infected cells is the RO, composed of large numbers of membranous structures seen on a low to medium power scan. Intracellular coronavirus is found singly or in groups within membrane-bound vacuoles and is unlikely to be found as an isolated virion in direct contact with the cytoplasm, in contrast to a clathrin-coated vesicle.

In conclusion, it is possible in the majority of cases to discriminate coronavirus from normal intracellular structures. A requirement for early collaboration between animal virus researchers and diagnostic clinical facilities is identified for future outbreaks of a novel virus to prevent interpretation errors and accelerate research.

Acknowledgements

Dr Roufosse is supported by the National Institute for Health Research (NIHR) Biomedical Research Centre based at Imperial College Healthcare NHS Trust and Imperial College London. The views expressed are those of the authors and not necessarily those of the NHS, the NIHR or the Department of Health. Infrastructure support for this research was provided by the NIHR Imperial Biomedical Research Centre. Dr Roufosse's research activity is made possible with generous support from Sidharth and Indira Burman, and with support from

Imperial College COVID19 research funds. We are grateful to the Centre for Ultrastructural Imaging at Guy's Campus for providing technical support.

Abbreviations

ACE2	angiotensin-converting enzyme 2
CCP	clathrin-coated pit
CCV	clathrin-coated vesicle
CGN	*cis*-Golgi network
COVID-19	coronavirus disease 2019
DMV	double membrane vesicle
E proteins	envelope proteins
EE	early endosome
EM	electron microscopy
ER	endoplasmic reticulum
ERGIC	endoplasmic reticulum-Golgi intermediate complex
ILV	intraluminal vesicle
LE	late endosome
M protein	membrane protein
MTOC	microtubule-organising centre
MVB	multivesicular body
N protein	nucleocapsid protein
NSP	non-structural protein
RE	recycling endosome
RO	replication organelle
RTC	replication transcription complex
SARS-CoV-2	severe acute respiratory syndrome coronavirus 2
S protein	spike protein
TGN	*trans*-Golgi network

Author contributions statement

DN, CR, CH, LM and EC conceived the project. LM and EC supplied electron micrographs. OS and WB supplied Vero cells infected and mock-infected with SARS-CoV2. LM, CR and BH were involved in the logistics, preparation, and assessment of the control and infected cultured cells. All the authors were involved in writing the paper and had final approval of the submitted and published versions.

References

1. Almeida JD, Tyrrell DA. The morphology of three previously uncharacterized human respiratory viruses that grow in organ culture. *J Gen Virol* 1967; **1:** 175–178.
2. Virology: coronaviruses. *Nature* 1968; **220:** 650.
3. Ding Y, Wang H, Shen H, *et al*. The clinical pathology of severe acute respiratory syndrome (SARS): a report from China. *J Pathol* 2003; **200:** 282–289.
4. Alsaad KO, Hajeer AH, Al Balwi BM, *et al*. Histopathology of Middle East respiratory syndrome coronovirus (MERS-CoV) infection – clinicopathological and ultrastructural study. *Histopathology* 2018; **72:** 516–524.
5. Baranov MV, Olea RA, van den Bogaart G. Chasing uptake: super-resolution microscopy in endocytosis and phagocytosis. *Trends Cell Biol* 2019; **29:** 727–739.
6. Calomeni E, Satoskar A, Ayoub I, *et al*. Multivesicular bodies mimicking SARS-CoV-2 in patients without COVID-19. *Kidney Int* 2020; **98:** 233–234.
7. Miller SE, Brealey JK. Visualization of putative coronavirus in kidney. *Kidney Int* 2020; **98:** 231–232.
8. Roufosse C, Curtis E, Moran L, *et al*. Electron microscopic investigations in COVID-19: not all crowns are coronas. *Kidney Int* 2020; **98:** 505–506.
9. Goldsmith CS, Miller SE, Martines RB, *et al*. Electron microscopy of SARS-CoV-2: a challenging task. *Lancet* 2020; **395:** e99.
10. Granger E, McNee G, Allan V, *et al*. The role of the cytoskeleton and molecular motors in endosomal dynamics. *Semin Cell Dev Biol* 2014; **31:** 20–29.
11. Weeratunga S, Paul B, Collins BM. Recognising the signals for endosomal trafficking. *Curr Opin Cell Biol* 2020; **65:** 17–27.
12. Gu F, Crump CM, Thomas G. Trans-Golgi network sorting. *Cell Mol Life Sci* 2001; **58:** 1067–1084.
13. Blott EJ, Griffiths GM. Secretory lysosomes. *Nat Rev Mol Cell Biol* 2002; **3:** 122–131.
14. Anelli T, Panina-Bordignon P. How to avoid a no-deal ER exit. *Cell* 2019; **8:** 1051.
15. Manzanares D, Ceña V. Endocytosis: the nanoparticle and submicron nanocompounds gateway into the cell. *Pharmaceutics* 2020; **12:** 371.
16. Elkin SR, Lakoduk AM, Schmid SL. Endocytic pathways and endosomal trafficking: a primer. *Wien Med Wochenschr* 2016; **166:** 196–204.
17. Kaksonen M, Roux A. Mechanisms of clathrin-mediated endocytosis. *Nat Rev Mol Cell Biol* 2018; **19:** 313–326.
18. Mayor S, Parton RG, Donaldson JG. Clathrin-independent pathways of endocytosis. *Cold Spring Harb Perspect Biol* 2014; **6:** a016758.
19. Maib H, Smythe E, Ayscough K. Forty years on: clathrin-coated pits continue to fascinate. *Mol Biol Cell* 2017; **28:** 843–847.
20. Ayloo S, Gu C. Transcytosis at the blood–brain barrier. *Curr Opin Neurobiol* 2019; **57:** 32–38.
21. Zhang X, Sessa WC, Fernández-Hernando C. Endothelial transcytosis of lipoproteins in atherosclerosis. *Front Cardiovasc Med* 2018; **5:** 130.
22. Hanson PI, Cashikar A. Multivesicular body morphogenesis. *Annu Rev Cell Dev Biol* 2012; **28:** 337–362.
23. Goldenring JR. Recycling endosomes. *Curr Opin Cell Biol* 2015; **35:** 117–122.
24. Huotari J, Helenius A. Endosome maturation. *EMBO J* 2011; **30:** 3481–3500.
25. Naslavsky N, Caplan S. The enigmatic endosome – sorting the ins and outs of endocytic trafficking. *J Cell Sci* 2018; **131:** jcs216499.
26. Gruenberg J. The endocytic pathway: a mosaic of domains. *Nat Rev Mol Cell Biol* 2001; **2:** 721–730.
27. Jovic M, Sharma M, Rahajeng J, *et al*. The early endosome: a busy sorting station for proteins at the crossroads. *Histol Histopathol* 2010; **25:** 99–112.
28. Tooze J, Hollinshead M. In AtT20 and HeLa cells brefeldin A induces the fusion of tubular endosomes and changes their distribution and some of their endocytic properties. *J Cell Biol* 1992; **118:** 813–830.
29. Simonetti B, Cullen PJ. Actin-dependent endosomal receptor recycling. *Curr Opin Cell Biol* 2019; **56:** 22–33.
30. Lu L, Hong W. From endosomes to the *trans*-Golgi network. *Semin Cell Dev Biol* 2014; **31:** 30–39.
31. Wenzel EM, Schultz SW, Schink KO, *et al*. Concerted ESCRT and clathrin recruitment waves define the timing and morphology of intraluminal vesicle formation. *Nat Commun* 2018; **9:** 2932.
32. Karim MA, Samyn DR, Mattie S, *et al*. Distinct features of multivesicular body-lysosome fusion revealed by a new cell-free content-mixing assay. *Traffic* 2018; **19:** 138–149.

33. Buratta S, Tancini B, Sagini K, *et al*. Lysosomal exocytosis, exosome release and secretory autophagy: the autophagic- and endo-lysosomal systems go extracellular. *Int J Mol Sci* 2020; **21:** 2576.
34. Papandreou ME, Tavernarakis N. Crosstalk between endo/exocytosis and autophagy in health and disease. *Biotechnol J* 2020; **15:** e900267.
35. Klionsky DJ, Eskelinen EL, Deretic V. Autophagosomes, phagosomes, autolysosomes, phagolysosomes, autophagolysosomes… Wait, I'm confused. *Autophagy* 2014; **10:** 549–551.
36. Inpanathan S, Botelho RJ. The lysosome signalling platform: adapting with the times. *Front Cell Dev Biol* 2019; **7:** 113.
37. Trivedi PC, Bartlett JJ, Pulinilkunnil T. Lysosomal biology and function: modern view of cellular debris bin. *Cells* 2020; **9:** 1131.
38. Martínez-Alonso E, Tomás M, Martínez-Menárguez JA. Morphofunctional architecture of the Golgi complex of neuroendocrine cells. *Front Endocrinol (Lausanne)* 2013; **4:** 41.
39. Raposo G, Stoorvogel W. Extracellular vesicles: exosomes, microvesicles, and friends. *J Cell Biol* 2013; **200:** 373–383.
40. Stahl AL, Johansson K, Mossberg M, *et al*. Exosomes and microvesicles in normal physiology, pathophysiology, and renal diseases. *Pediatr Nephrol* 2019; **34:** 11–30.
41. Meckes DG Jr, Raab-Traub N. Microvesicles and viral infection. *J Virol* 2011; **85:** 12844–12854.
42. Kabachinski G, Schwartz TU. The nuclear pore complex – structure and function at a glance. *J Cell Sci* 2015; **128:** 423–429.
43. Rhodin JAG. *Histology. A Text and Atlas*. Oxford University Press: New York, 1974; 7–64.
44. Ghadially FM. *Ultrastructural Pathology of the Cell and Matrix, Volume 2*, (4th edn); chapter 16. Butterworth-Heinemann: Boston, 1997; 1207–1306.
45. Snijder EJ, Limpens RWAL, de Wilde AH, *et al*. A unifying structural and functional model of the coronavirus replication organelle: tracking down RNA synthesis. *PLoS Biol* 2020; **18:** e3000715.
46. Neuman BW, Adair BD, Yoshioka C, *et al*. Supramolecular architecture of severe acute respiratory syndrome coronavirus revealed by electron cryomicroscopy. *J Virol* 2006; **80:** 7918–7928.
47. Caly L, Druce J, Roberts J, *et al*. Isolation and rapid sharing of the 2019 novel coronavirus (SARS-CoV-2) from the first patient diagnosed with COVID-19 in Australia. *Med J Aust* 2020; **212:** 459–462.
48. Fung TS, Liu DX. Human coronavirus: host–pathogen interaction. *Annu Rev Microbiol* 2019; **73:** 529–557.
49. Knoops K, Kikkert M, Worm SH, *et al*. SARS-coronavirus replication is supported by a reticulovesicular network of modified endoplasmic reticulum. *PLoS Biol* 2008; **6:** e226.
50. Letko M, Marzi A, Munster V. Functional assessment of cell entry and receptor usage for SARS-CoV-2 and other lineage B betacoronaviruses. *Nat Microbiol* 2020; **5:** 562–569.
51. Ou X, Liu Y, Lei X, *et al*. Characterization of spike glycoprotein of SARS-CoV-2 on virus entry and its immune cross-reactivity with SARS-CoV. *Nat Commun* 2020; **11:** 1620.
52. Hoffmann M, Kleine-Weber H, Schroeder S, *et al*. SARS-CoV-2 cell entry depends on ACE2 and TMPRSS2 and is blocked by a clinically proven protease inhibitor. *Cell* 2020; **181:** 271–280.
53. Shang J, Wan Y, Luo C, *et al*. Cell entry mechanisms of SARS-CoV-2. *Proc Natl Acad Sci U S A* 2020; **117:** 11727–11734.
54. Gheblawi M, Wang K, Viveiros A, *et al*. Angiotensin-converting enzyme 2: SARS-CoV-2 receptor and regulator of the renin–angiotensin system: celebrating the 20th anniversary of the discovery of ACE2. *Circ Res* 2020; **126:** 1456–1474.
55. Wang H, Yang P, Liu K, *et al*. SARS coronavirus entry into host cells through a novel clathrin- and caveolae-independent endocytic pathway. *Cell Res* 2008; **18:** 290–301.
56. Yang N, Shen HM. Targeting the endocytic pathway and autophagy process as a novel therapeutic strategy in COVID-19. *Int J Biol Sci* 2020; **16:** 1724–1731.
57. Norris A, Grant BD. Endosomal microdomains: formation and function. *Curr Opin Cell Biol* 2020; **65:** 86–95.
58. Angelini MM, Akhlaghpour M, Neuman BW, *et al*. Severe acute respiratory syndrome coronavirus nonstructural proteins 3, 4, and 6 induce double-membrane vesicles. *mBio* 2013; **4:** e00524–e00513.
59. Blanchard E, Roingeard P. Virus-induced double-membrane vesicles. *Cell Microbiol* 2015; **17:** 45–50.
60. Snijder EJ, van der Meer Y, Zevenhoven-Dobbe J, *et al*. Ultrastructure and origin of membrane vesicles associated with the severe acute respiratory syndrome coronavirus replication complex. *J Virol* 2006; **80:** 5927–5940.
61. van Hemert MJ, van den Worm SH, Knoops K, *et al*. SARS-coronavirus replication/transcription complexes are membrane-protected and need a host factor for activity *in vitro*. *PLoS Pathog* 2008; **4:** e1000054.
62. Hagemeijer MC, Monastyrska I, Griffith J, *et al*. Membrane rearrangements mediated by coronavirus nonstructural proteins 3 and 4. *Virology* 2014; **458–459:** 125–135.
63. Reggiori F, de Haan CA, Molinari M. Unconventional use of LC3 by coronaviruses through the alleged subversion of the ERAD tuning pathway. *Viruses* 2011; **3:** 1610–1623.
64. Zhu N, Zhang D, Wang W, *et al*. A novel coronavirus from patients with pneumonia in China, 2019. *N Engl J Med* 2020; **382:** 727–733.
65. Malik YA. Properties of coronavirus and SARS-CoV-2. *Malays J Pathol* 2020; **42:** 3–11.
66. Goldsmith CS, Miller SE. Modern uses of electron microscopy for detection of viruses. *Clin Microbiol Rev* 2009; **22:** 552–563.
67. Martines RB, Ritter JM, Matkovic E, *et al*. Pathology and pathogenesis of SARS-CoV-2 associated with fatal coronavirus disease, United States. *Emerg Infect Dis* 2020; **26:** 2005–2015.
68. Harcourt J, Tamin A, Lu X, *et al*. Severe acute respiratory syndrome coronavirus 2 from patient with 2019 novel coronavirus disease, United States. *Emerg Infect Dis* 2020; **26:** 1266–1273.
69. Miller SE. Detection and identification of viruses by electron microscopy. *J Electron Microsc Tech* 1986; **4:** 265–301.
70. Miller SE. Problems and pitfalls in diagnostic electron microscopy. *Microsc Microanal* 2012; **18:** 172–173.
71. Fassel TA, Raisch KP, Chetty N, *et al*. Ruthenium red preserves glycoprotein peplomers of C-type retroviruses for transmission electron microscopy. *Biotech Histochem* 1998; **73:** 222–227.
72. Goldsmith CS, Tatti KM, Ksiazek TG, *et al*. Ultrastructural characterization of SARS coronavirus. *Emerg Infect Dis* 2004; **10:** 320–326.
73. Das Murtey M. Immunogold techniques in electron microscopy. In *Modern Electron Microscopy in Physical and Life Sciences*, Janecek M, Kral R (eds). London: IntechOpen, 2016; 143–160. https://doi.org/10.5772/61719.
74. Mizuiri S, Ohashi Y. ACE and ACE2 in kidney disease. *World J Nephrol* 2015; **4:** 74–82.
75. Hamming I, Cooper ME, Haagmans BL, *et al*. The emerging role of ACE2 in physiology and disease. *J Pathol* 2007; **212:** 1–11.
76. Chai X, Hu L, Zhang Y, *et al*. Specific ACE2 expression in cholangiocytes may cause liver damage after 2019-NCoV infection. *bioRxiv* 2020. https://doi.org/10.1101/2020.02.03.931766. Not peer reviewed.
77. Hamming I, Timens W, Bulthuis ML, *et al*. Tissue distribution of ACE2 protein, the functional receptor for SARS coronavirus. A first step in understanding SARS pathogenesis. *J Pathol* 2004; **203:** 631–637.
78. Baig AM, Khaleeq A, Ali U, *et al*. Evidence of the COVID-19 virus targeting the CNS: tissue distribution, host–virus interaction, and proposed neurotropic mechanisms. *ACS Chem Nerosci* 2020; **11:** 995–998.
79. Bradley BT, Maioli H, Johnston R, *et al*. Histopathology and ultrastructural findings of fatal COVID-19 infections in Washington State: a case series. *Lancet* 2020; **396:** 320–332.

80. Schaefer I-M, Padera RF, Solomon IH, *et al*. *In situ* detection of SARS-CoV-2 in lungs and airways of patients with COVID-19. *Mod Pathol* 2020. https://doi.org/10.1038/s41379-020-0595-z
81. Adachi T, Chong J-M, Nakajima N, *et al*. Clinicopathologic and immunohistochemical findings from autopsy of patient with COVID-19, Japan. *Emerg Infect Dis* 2020; **26:** 2157–2161.
82. Dorward D, Russell CD, Um IH, *et al*. Tissue-specific tolerance in fatal Covid-19. *medRxiv* 2020. https://doi.org/10.1101/2020.07.02.20145003. Not peer reviewed.
83. Menter T, Haslbauer JD, Ninehold R, *et al*. Postmortem examination of COVID-19 patients reveals diffuse alveolar damage with severe capillary congestion and variegated findings of lungs and other organs suggesting vascular dysfunction. *Histopathology* 2020; **77**: 198–209.
84. Puelles VG, Jutgehetmann M, Lindenmeyer MT, *et al*. Multiorgan and renal tropism of SARS-CoV-2. *N Engl J Med* 2020; **383:** 590–592.
85. Lindner D, Fitzek A, Bräuninger H, *et al*. Association of cardiac infection with SARS-CoV-2 in confirmed COVID-19 autopsy cases. *JAMA Cardiol* 2020: e203551. https://doi.org/10.1001/jamacardio.2020.3551
86. Colmenero I, Santonja C, Alonso-Riaño M, *et al*. SARS-CoV-2 endothelial infection causes COVID-19 chilblains: histopathological, immunohistochemical and ultrastructural study of seven paediatric cases. *Br J Dermatol* 2020; **183**: 729–737.